# Scanner-based Measurement of Print Line Placement

*Suhail S. Saquib, Dirk W. Hertel, James W. Slack, Brian Busch, and Richard G. Egan*
*Polaroid Corporation*
*Waltham, Massachusetts*

## Abstract

Exact placement of print lines is extremely important to reduce density banding and color misregistration in a high-speed thermal tandem printer that employs separate print stations for each color. We propose a flatbed scanner method for precisely estimating the errors of line placement and print velocity. Our approach uses a model for the scanned data that translates line placement errors into phase variations. A classical phase estimation algorithm is then employed to robustly estimate the line placement error in the presence of print artifacts such as noise and thermal history effects. The optical distortion of the flatbed scanner is measured and the spatial frequency bands that contain large scanner errors are excluded from the analysis of the printer. We present examples that show the usefulness of this method in identifying problems in printer transport systems, and in verifying the effectiveness of solutions to these problems.

## Introduction

The exact placement of print lines is extremely important to avoid print artifacts. Any variation in the relative velocity between the line printing device (e.g. a linear thermal print-head) and the print media causes variations in both the distance between print lines and exposure (e.g. energy per area in a thermal printing system). Both effects lead to 'banding', a variation in print density which is correlated in the direction of the linear print head, and therefore highly visible compared to an isotropic random density variation of the same magnitude (e.g. film granularity). In variable dot halftoned systems, velocity variation results not only in dot placement variations but also in dot size fluctuations. In color printing, velocity variation results in misregistration between the colors, causing color banding if the halftone screens are not designed properly.

The control of print line placement is especially important in tandem color printers.[1] High-resolution drum scanners have been used in the past to measure line placement errors in laser printing and to optimize closed-loop velocity controls.[2,3] A high-resolution CCD line camera with an encoder-controlled scanning stage has been proposed as a means for measuring line placement errors in the micrometer range.[4] However, such equipment is costly and measurement time still too long for routine testing. Flatbed scanners offer shorter measurement times and are comparatively lower in cost, but they introduce large errors: a random motion error in the slow scan direction, and optical distortion in the fast-scan direction. The optical distortion error can be corrected when measuring against reference marks printed by a high-precision printer alongside the test image.[5] However, this method may be undesirable for several reasons. First, the reference lines of the calibration target printed on the test media may get distorted during printing due to heat or tension. Second, it may not be possible to print reference lines on the test media. Third, the precision and resolution of the reference printer limit the accuracy of the method. In view of the above drawbacks, we propose instead an off-line measurement of the optical distortion of the scanner using a high-precision line target. The spatial frequency bands that carry large scanner errors are subsequently excluded from the analysis of the printer transport system. The estimation of line placement and velocity error is accomplished by formulating a model for the scanned data.

## Data Model

The placement error of print lines in the media transport direction is determined by printing a test image containing equally spaced lines on the printer to be analyzed. The print is scanned using a flatbed scanner, with the print lines oriented perpendicular to the CCD line array of the scanner. The scanned image of the print is then averaged perpendicular to the print lines to produce a 1-D signal $y$. In a print free of line placement errors, the 1-D signal could be approximately modeled as an ideal sine wave of frequency $f$, where $f$ is the number of lines printed per mm. However, line placement errors produced by non-uniform media motion results in a variable phase $\phi$ of the ideal sine wave. Therefore, an appropriate model for the scanned 1-D signal is given as

$$y = A(x)\sin(2\pi fx + \phi(x)). \quad (1)$$

where $x$ is the distance measured in the transport direction in mm and $A$ is the amplitude. Note that $A$ is a function of $x$ to account for any density variations that might occur due to velocity variation and thermal history effects in thermal printers.

Let $e(x)$ be the line placement error in mm, interpreted as the distance between the printed line and the corresponding virtual line of an ideal printer printing $f$ lines per mm with no velocity variations. Since a phase change of $2\pi$ corresponds to a line placement error equal to the pitch of the sine wave, $1/f$, it follows that

$$e(x) = \frac{-\phi(x)}{2\pi f}.. \tag{2}$$

The sign convention is that a negative error implies the printed line is placed before its intended position and vice versa. Let $v$ be the velocity of the ideal printer and $\Delta v(x)$ be the velocity error of the real printer with respect to the ideal printer. Then the fractional velocity error is given as

$$\frac{\Delta v(x)}{v} = \frac{d}{dx} e(x) \tag{3}$$

## Line Frequency Estimation

Before the line placement error is determined, the line frequency $f$ needs to be estimated. It is desirable to estimate $f$ directly from the scanned signal $y$ rather than using *a priori* knowledge of the printer resolution since errors in the scanner pitch might alter the line frequency in the observed signal $y$. A robust way of estimating $f$ is computing the Fourier power spectrum of the signal $y$ and choosing the line frequency $f$ to be the frequency where the computed power spectrum peaks. Any error in the estimation of this frequency manifests itself in the final phase estimate as a linear trend. It follows from Eq. (1) that the estimated phase is related to the true phase as follows

$$\hat{\phi}(x) = \phi(x) + 2\pi\Delta f x \tag{4}$$

where $\Delta f$ is the error in estimating $f$. The residual frequency error $\Delta f$ is estimated by computing the slope of a straight line fit to the phase estimate. The straight line fit is then subtracted from the phase estimate to obtain the corrected phase estimate.

## Phase Estimation

In this Section, we derive an estimate of phase $\phi(x)$ given the observed signal $y$. The technique is similar to that in a classical phase lock loop.[6] Without loss of generality, the following analysis assumes that the frequency $f$ has been estimated accurately, i.e. $\Delta f = 0$, since the procedure outlined in the previous Section can be used to remove the effect of any residual frequency error.

To isolate the phase $\phi(x)$ from the observed signal, we multiply $\phi(x)$ with a sine and a cosine wave of frequency $f$. Let

$$\begin{aligned} c(x) &= y\sin(2\pi fx) \\ &= \frac{A(x)}{2}\left[\cos(\phi(x)) - \cos(4\pi fx + \phi(x))\right] \end{aligned} \tag{5}$$

and

$$\begin{aligned} s(x) &= y\cos(2\pi fx) \\ &= \frac{A(x)}{2}\left[\sin(\phi(x)) + \sin(4\pi fx + \phi(x))\right] \end{aligned} \tag{6}$$

We are interested in separating the two terms in Eqs. (5) and (6). Since the bandwidth of $\phi(x)$ is determined by the characteristics of the media transport system of the printer, the first term in both $c(x)$ and $s(x)$ will typically be restricted to low frequencies. Therefore, by choosing the printed line frequency $f$ to be sufficiently high, we can separate the two terms in Eqs. (5) and (6) on the frequency axis by using a low-pass filter. The design considerations for such a filter is dealt with in the next Section.

Let $LPF[\cdot]$ denote a low-pass filter operator. Using Eqs. (5) and (6), we obtain the phase estimate as

$$\hat{\phi}(x) = \tan^{-1}\left(\frac{LPF[s(x)]}{LPF[c(x)]}\right) \tag{7}$$

Note that since the phase estimate is computed from a ratio of the filtered signals $c(x)$ and $s(x)$, the estimate is quite robust to low frequency amplitude variations $A(x)$ present in signal $y$. Figure 1 shows the block diagram of the phase estimator. In practice, any inaccuracies in the estimation of the line frequency $f$ will result in phase wrapping. Therefore, the phase estimate given by Eq. (7) needs to be unwrapped and the residual frequency error $\Delta f$ removed from it before the line placement and velocity errors given by Eq. (2) and (3) are computed.

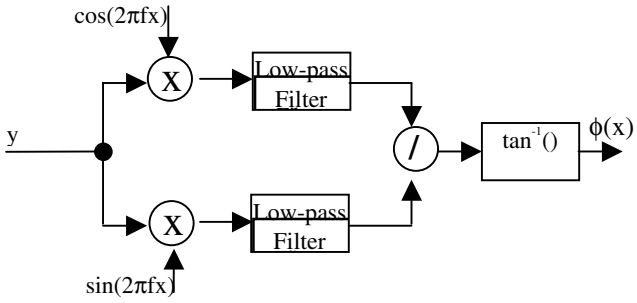


*Figure 1. Block diagram of phase estimator*

In the interest of simplicity, we have not taken into account the effect of noise on the phase estimate in our analysis. However, if we had included an additive white Gaussian noise term in our data model given by Eq. (1), the phase estimate of Eq. (7) would also be the maximum likelihood estimate.[7]

## Detector Filter Design Considerations

The role of the low-pass detector filter as outlined in the previous Section is to separate the low- and high-frequency terms in Eqs. (5) and (6). To avoid any phase distortion in the filtered result, we employ a linear phase finite impulse response (FIR) filter for this purpose.

Let $2B$ be the bandwidth of either of the terms $\cos(\phi(x))$ or $\sin(\phi(x))$. The high frequency terms in Eqs. (5) and (6) then occupy the frequency range $[2f\text{-}B, 2f\text{+}B]$, as shown in Fig. 2. Consequently, the low-pass filter should attenuate all frequencies above $2f\text{-}B$. Furthermore, the filter needs to pass all frequencies below $B$ to ensure the low frequency terms $\cos(\phi(x))$ and $\sin(\phi(x))$ remain untouched. This allows the transition bandwidth $\delta$ of the filter to be $\delta = 2(f\text{-}B)$. To ensure that $\delta > 0$, it is required that we choose $f > B$. Note that the spatial support of the FIR filter grows larger as $\delta$ becomes smaller. Therefore it is desirable to have $f >> B$, allowing for a reasonably large transition bandwidth for the low-pass filter. Figure 2 illustrates the filter design parameters.

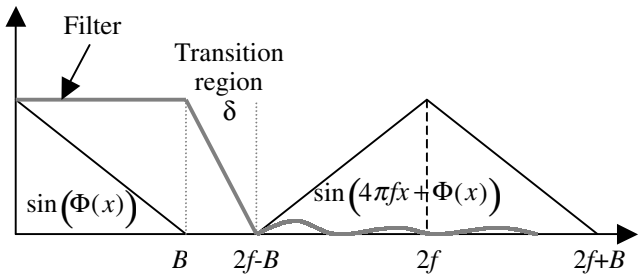


*Figure 2. The pass-, transition- and stop-band of the low-pass phase detector filter are shown above for separating the two terms in Eq. (5). Similar design considerations hold for Eq. (6).*

Note that for a digital implementation of the phase detector, the sampling frequency should be chosen to be greater than $4f\text{+}2B$ to avoid any aliasing artifacts since the highest frequency in the phase estimation procedure will be $2f\text{+}B$.

## Pre-Processing Data

Any mismatch between our assumed data model given by Eq. (1) and the data will result in erroneous phase estimation. For example, if the printer to be analyzed is a thermal printer, the measured data has some low frequency content due to thermal history effects.[8] The source of this low frequency content is the gradual heating of the heat-sink of the thermal printer that results in increasing density as the printing proceeds. Fortunately, this undesirable low frequency signal can be easily isolated on the frequency axis from our signal of interest $\phi(x)$, which is centered around the higher line frequency $f$. This isolation is achieved by filtering the scanned data with a band-pass filter that passes all frequencies from $f\text{-}B$ to $f\text{+}B$. Again, a linear phase FIR filter is employed for this purpose to avoid any phase distortion in the filtered data. Note that this pre-filter also eliminates any noise outside the frequency band of interest and makes the filtered data band-limited and consistent with our proposed model of Eq. (1).

## Flatbed Scanner Error

Figure 3 illustrates the superposition of scanner error and printer line placement error. The only way to distinguish between the two is to measure the scanner pitch error with a high-precision line calibration target.

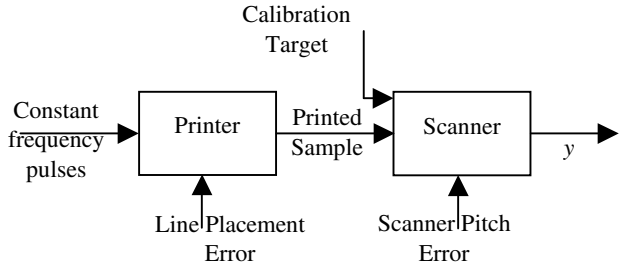


*Figure 3. The signal y has errors arising from both the printer and the scanner. The only way to distinguish the two errors is to scan a calibration target along with the print sample.*

The analysis of a population of ten scanners (UMAX PowerLook III) showed that optical distortion varied not only between units, but also from top to bottom of each scanner platen. Therefore an exact scanner calibration with a high-precision target was found to be impractical because it would have to be in absolute scanner coordinates, only valid for a particular unit, and still not precise enough when variations in time occur.

The analysis of the above ten scanner units showed that the spectral power of the scanner pitch error was concentrated at spatial frequencies below 0.2 cycles/mm. The rms scanner error in frequency bands greater than 0.2 cycles/mm was on the order of 0.05 μm, which was very much smaller than the printer error we were dealing with. We could therefore successfully separate the scanner distortion from the print line placement error by excluding all frequencies below 0.2 cycles/mm from our printer analysis.

## Results

We present experimental results on thermal printers that demonstrate the value of the scanner-based tool for analyzing dot placement accuracy of the media transport. This analysis is useful in both identifying motion problems and verifying how effective proposed solutions are in addressing those problems.

All the results presented here are for an experimental high-speed tandem printer with four print stations for cyan, magenta, yellow, and overcoat. We assumed $B$=7.5 cycles/mm for the transport system of this printer. We printed cyan monochrome samples with equally spaced lines at a resolution of 200 dpi. A UMAX PowerLook III scanner was used to scan the print sample at 1200 dpi. The sampling rate, after averaging the scan along the lines, was increased to 2400 dpi by linear interpolation. We estimated $f$ from the power spectrum to be 7.86 lines/mm. A pre-filter with transition bands [1.0,1.25] and [15.36,19.36] and a

pass-band of [1.25,15.36] cycles/mm was applied to the scanned data. The transition band of the phase detector low-pass filter was set to [7.5,8.21] cycles/mm. Figure 4 shows the magnitude, and phase response of this FIR filter (order 296), which was designed using the Kaiser window.

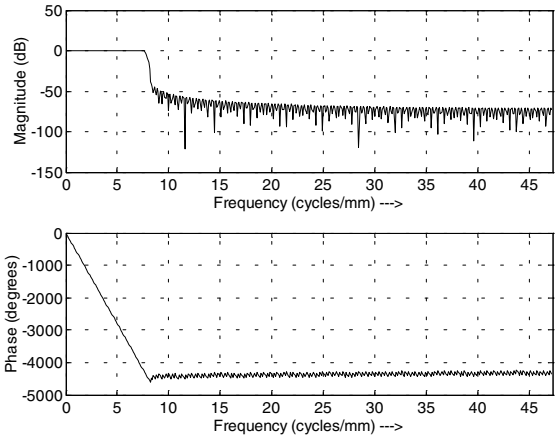


*Figure 4. The magnitude and phase response of the low-pass phase detector filter.*

Figure 5 shows the power spectrum of the estimated line placement error computed with a frequency resolution of 0.023 cycles/mm. Note that the high power in frequencies less than 0.2 cycles/mm is attributed to optical distortion of the scanner. We also see strong peaks in the spectrum at 0.78, 1.56, 3.15 and 4.7 cycles/mm. A two phase, 400 steps/revolution stepper motor was used to drive the media. Since the circumference of the capstan drive roller was 63.5 mm, the highest step frequency of the stepper motor on the media was 6.3 cycles/mm. Since the peaks at 0.78, 1.56 and 3.15 cycles/mm are sub-harmonics of 6.3 cycles/mm, it implicates the drive stepper motor as the source of this banding problem. In another instance, a particular design of the media transport system resulted in highly visible banding at 0.25 cycles/mm. The line placement error was estimated from a print sample using the same machine settings as described above. The estimated line placement error was then filtered using a narrow band-pass filter with [0.2,0.5] cycles/mm as its pass-band. The filtered placement error and percentage velocity variation is shown in Fig. 6(a). We observe that peak-to-peak placement error is close to 10 μm and the rms variation is 1.69 μm. The problem was traced to a natural resonance of the donor transport system. Any excitation from the media transport would set this system into oscillations resulting in severe visible banding. Fig. 6(b) shows that a re-designed donor transport system with active tension control and viscous damping improved the dot placement accuracy significantly, with peak-to-peak placement error of about 5 μm and the rms variation reduced to 0.36 μm.

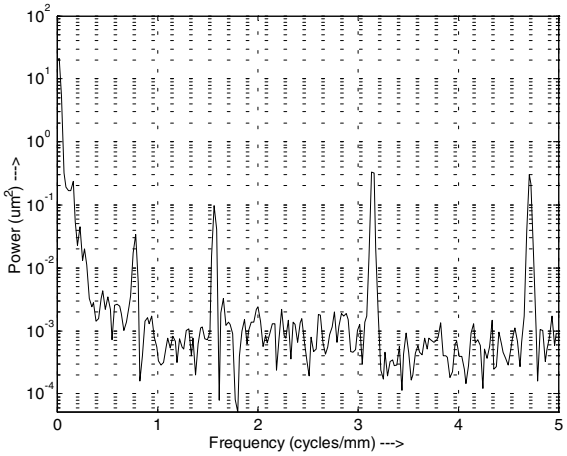


*Figure 5. Power spectrum of the estimated line placement error for the high speed tandem thermal printer. Strong peaks are seen at 0.78, 1.56, 3.15 and 4.7 cycles/mm.*

## Conclusion

We have presented a fast model-based estimation method for analyzing the line placement and velocity error of the transport system of any printer. Our method has several advantages. First, the model-based approach is robust to noise and density variations in the print. Second, the use of a flatbed scanner results in low equipment cost and short measurement times. The power spectrum of the scanner pitch error is first computed to determine which frequency bands have high power. These frequency bands are subsequently excluded when analyzing printers. We demonstrated the utility of this tool in transport system problem identification and verification of effectiveness of proposed solutions.

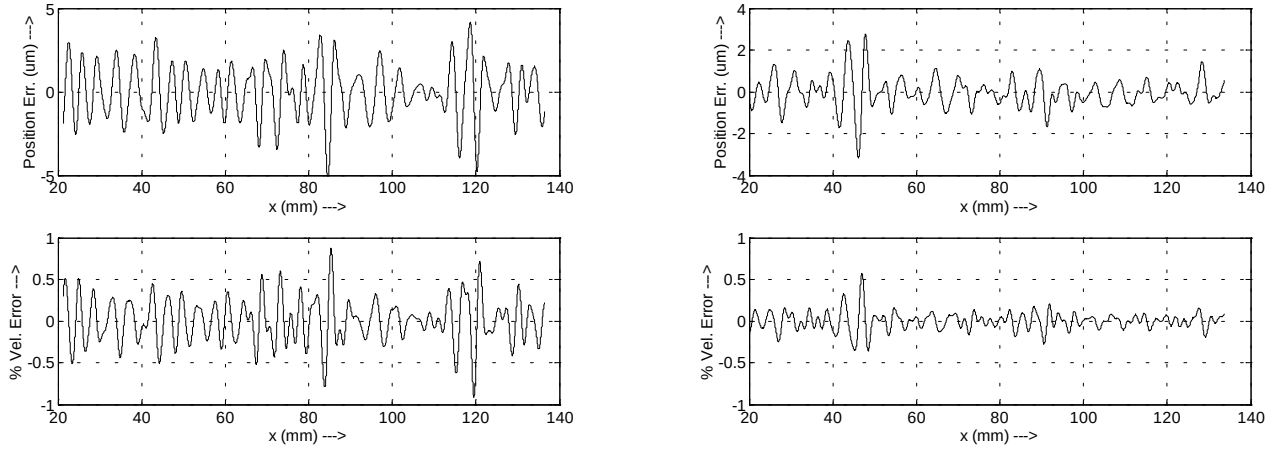


(a) (b)

*Figure 6. The line placement and percentage velocity error of a high speed tandem thermal printer in the frequency band [0.2, 0.5] cycles/mm is shown above. (a) Here the transport system of the printer suffers from a resonance at 0.25 cycles/mm. (b) Improved transport system that has active tension control on donor unwind and take-up and damping on the receiver unwind system.*

## References

1. T. Kusuda, M. Ikeda, T. Ogiri, T. Besshi, Transmission Deviation Caused by Eccentricity in Multi Gear Systems, *Proc. PICS*, pg. 119. (1999).
2. G-Y. Liny, J. M. Gricey, J. P. Allebach, G. Chiuz , Banding Artifact Reduction in Electrophotographic Printers by Using Pulse Width Modulation, *Proc. NIP16*, pg. 281.(2000).
3. C-L. Chen, G. T.-C. Chiu, J. P. Allebach, Banding Artifact Reduction in Electrophotographic Processes Using OPC, *Proc. NIP17*, pg. 60. (2001).
4. Y. Kipman, K. Johnson, Dot Placement Analysis using a Line Scan Camera and Rigid Body Rotation, *Proc. PICS*, pg.68. (2001).
5. M. C. Mongeon, E. Dalal, R. Rasmussen, Utilizing Flatbed Scanners to Measure Printer Motion Quality Error, *Proc. PICS*, pg. 387. (2001).
6. J. P. Costas, Synchronous Communications, *Proc. IRE*, vol. **44,** pg. 1713-1718. (1956).
7. J. G. Proakis, *Digital Communications*, McGraw-Hill, NY, pg. 324. (1989).
8. S. S. Saquib, W. Vetterling, Model-Based Thermal History Control, *Proc. NIP18*, p. 200 (2002).

## Biographies

**Suhail S. Saquib** received his B.Tech. degree in Electronics and Electrical Communication Engineering from Indian Institute of Technology, Kharagpur, India, in 1991. He received his M.S. and Ph.D. degrees from Purdue University in 1992 and 1997 respectively. During the summer of 1996, he worked at Los Alamos National Laboratories in the area of medical optical tomography. Since 1997 he has been a member of the Image Science Lab. at Polaroid Corporation. His interests include ill-posed inverse problems, model-based image reconstruction techniques, numerical methods, tomography, and pattern recognition.

**Dirk Hertel** gained his physics degree (1979), and a Ph.D. (1989) for research work on the measurement and interpretation of microfilm image quality from the Technical University Dresden (Germany). He worked at the TU Dresden as assistant lecturer in imaging science, and researcher specializing in computer modeling and the microdensitometry of photographic image quality. Since joining Polaroid Corporation in 1998 he has developed scanner-based print evaluation tools and worked on optimizing image quality in digital print media and hardware.